


Coupled localized surface plasmon resonances in periodic arrays of gold nanowires on ion-exchange waveguide technology

Ricardo Tellez-Limon¹ , Florent Gardillou², Victor Coello³ and Rafael Salas-Montiel⁴

¹ CONACYT—Centro de Investigación Científica y de Educación Superior de Ensenada, B. C., Unidad Monterrey, Alianza Centro 504, PIIT, 66629 Apodaca Nuevo León, Mexico

² Teem Photonics, 61 chemin du Vieux Chêne, Meylan F-38240, France

³ Centro de Investigación Científica y de Educación Superior de Ensenada, B. C., Unidad Monterrey, Alianza Centro 504, PIIT, 66629 Apodaca Nuevo León, Mexico

⁴ Department of Physics, Mechanics, Materials and Nanotechnology, L2n CNRS ERL 7004, Université de Technologie de Troyes, 10004 Troyes, France

E-mail: rtellez@conacyt.mx and rafael.salas@utt.fr

Received 28 August 2020, revised 10 November 2020

Accepted for publication 2 December 2020

Published 12 January 2021



Abstract

Coupled localized surface plasmon resonances (LSPRs) in periodic arrays of metallic nanowires are attractive for use in sensing applications due to their light enhancement and their sensitivity to the surrounding environment. Due to the interwire coupling, they behave as plasmonic waveguides with high wavevector modes that require bulky methods for efficient excitation. In this contribution, we demonstrate the excitation of coupled LSPRs in gold nanowires with photonic modes supported by an optical waveguide made with ion exchange technology. Currently, although weakly-coupled LSPRs are experimentally demonstrated, strongly-coupled LSPRs are only demonstrated numerically due to the challenge represented by the fabrication of a high density nanowire array with current electron beam lithography. Due to their operation across the visible spectrum and its low-loss coupling to standard optical fibers, integrated nanowires on glass waveguides open new perspectives for the development of hybrid photonic-plasmonic integrated optical devices.

Keywords: integrated optics, plasmonics, nanowires, near-field optics

(Some figures may appear in colour only in the online journal)

1. Introduction

Generally, the field of plasmonics is associated with two types of collective free electron oscillations in metals known as surface plasmon polaritons (SPPs) and localized surface plasmons (LSPs). While SPPs are usually referred to as surface waves propagating at a dielectric–metal interface, LSPs are nonpropagating excitations in metallic nanoparticles (MNPs) embedded in a dielectric environment [1]. In addition to these two types of plasmonic oscillations, plasmonic chain modes can be generated in a linear chain of closely spaced

MNPs [2] and nanowires [3]. Hybrid plasmon polaritons, composed of LSPs and SPPs also exist in a chain of MNPs situated on a layered medium [4, 5]. Chain modes can be described as coupled localized surface plasmon resonances (LSPRs) [4, 6–8] and therefore, are sensitive to environmental variations in the same manner as noncoupled LSPRs. The exploitation of LSPRs in periodic arrays of MNPs had thus attracted the interest of scientists and engineers for sensing applications, as well as being used in optical communications and solar cells, among many other applications [9–14]. An ultimate aim is to implement plasmonic circuits that

integrate different components into a single device. However, coupled LSPRs suffer from metallic loss that hinders their potential for many applications. In this sense, the integration of plasmonic arrays of metallic nanowires with dielectric optical waveguides becomes an attractive approach. These hybrid photonic-plasmonic systems provide an efficient excitation of coupled LSPRs in chains of MNPs [15] and metallic nanowires with different cross sections [16, 17]. For applications across the visible spectrum, different platforms for photonic integrated circuits have been proposed such as lithium niobate [18] and silicon nitride [19] waveguides. However, due to their aspect ratio and high index contrast between their core and surrounding media, these waveguides suffer from modal birefringence as well as high coupling loss [20]. An interesting alternative to such platforms is ion-exchange waveguide technology for the excitation of plasmonic modes [21]. Ion-exchanged waveguides (IExWGs) can operate across the visible spectrum, present low propagation loss, low birefringence, and are fully compatible with commercial optical fibers [22].

In this work, we demonstrate the excitation of coupled LSPRs in a periodic array of gold nanowires integrated on top of an IExWG on glass across the visible spectrum. We describe the operation principle of the integrated device with emphasis on the eigenmode analysis of the periodic array of metallic nanowires. Strongly, as well as weakly, coupled LSPRs are numerically calculated and plotted in proper dispersion relation plots and field propagation. Additionally, we describe the fabrication and characterization of the integrated periodic array of metallic nanowires on the IExWG. Far- and near-field regimes were characterized with the use of transmission spectroscopy and near-field scanning optical microscopy (NSOM) techniques. Coupled LSPRs can be achieved with periods shorter than $\lambda/2n_{\text{eff}}$. Currently, the fabrication of a periodic array of nanowires with a width of 75 nm and a period shorter than 120 nm is not attainable systematically with standard electron beam lithography (EBL) techniques.

2. Methods and materials

2.1. Description and principle of operation of the structure

The structure consists of a subwavelength periodic array of gold nanowires (AuNW) fabricated on top of an IExWG on glass (figure 1(a)). The size of each nanowire is $w = 75$ nm along the z -axis, $h = 30$ nm in height, and invariant along the y -axis. The structure has a discrete translational symmetry in the z direction with period Λ (figure 1(b)). To control the mode coupling and to facilitate fabrication, an intermediate layer of indium tin oxide (ITO) of thickness $t_{\text{ITO}} = 20$ nm is placed between the plasmonic and photonic waveguides ($n_{\text{ITO}} = 1.9$).

The principle of operation of the hybrid plasmonic/photonic structure is based on the mode coupling between the array mode, which results from the coupled LSPRs in the periodic array, and the photonic mode of the IExWG. The array mode can then be excited with the photonic mode of the IExWG with proper phase matching conditions. The

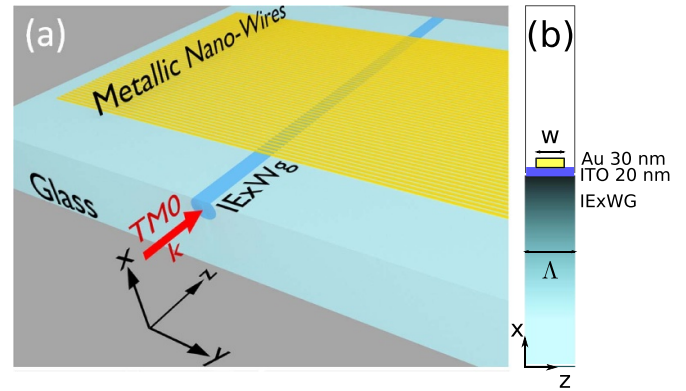


Figure 1. Coupled LSPRs in a periodic array of gold nanowires on IExWG technology. (a) Schematic representation of the structure and its excitation. (b) Schematic of a unit cell of the structure with discrete translational symmetry of period Λ . The nanowires are invariant along the y -axis while the IExWG is confined along the xy plane. A ITO layer is placed between the metallic nanowires and the IExWG.

array mode results from the discrete translational symmetry of the array and therefore leads to the conservation of the wave vector. This wave vector should match the wave vector of the IExWG mode. As the length of the nanowires is in the order of tens of micrometers, they are considered as invariant along the y direction. Hence, the LSP resonances only depend on their nanometric cross section. For the current cross section, only the TM mode is expected to excite array modes.

The optical modes supported by ion exchange waveguides are completely index guiding modes. It is straightforward to obtain the dispersion relation of an IExWG with the use of mode solvers provided that the index profile distribution is available. This distribution is assumed to be linearly proportional to the concentration profile of ions $C(x, y)$ involved in the ion exchange process as:

$$n(x, y, \lambda) = n_{\text{sub}}(\lambda) + \Delta n_0(\lambda)C(x, y), \quad (1)$$

where $n_{\text{sub}}(\lambda)$ is the refractive index of the substrate, and $\Delta n_0(\lambda)$ is an experimental value related to the maximum increase of refractive index that can be achieved with a maximum ion concentration (i.e. $C = 1$). The index distribution is thus controlled by the concentration profile. The dynamics of the ion concentration profile is in turn governed by the diffusion equation (9) in [23]. Using finite difference methods, we numerically solved this equation with the following parameters: 20% silver ions (Ag^+), exchange temperature $T = 603$ K, exchange time $t = 4$ min, and $\Delta n_0(\lambda) = 0.08$. The diffusion parameters were $D_{\text{Ag}} = 1.3 \times 10^{-15} \text{ m}^2 \text{ s}^{-1}$, $\alpha = 0.9$ [24], and the ion diffusion window was $1.5 \mu\text{m}$. We then used MODE solutions solver by Lumerical to calculate the dispersion relation of guided modes. To calculate the dispersion relation of the periodic array of gold nanowires ($\Lambda = 185$ nm), we used the finite-difference time-domain method FDTD solutions by Lumerical, as described in [25]. Here, a unit cell was used in

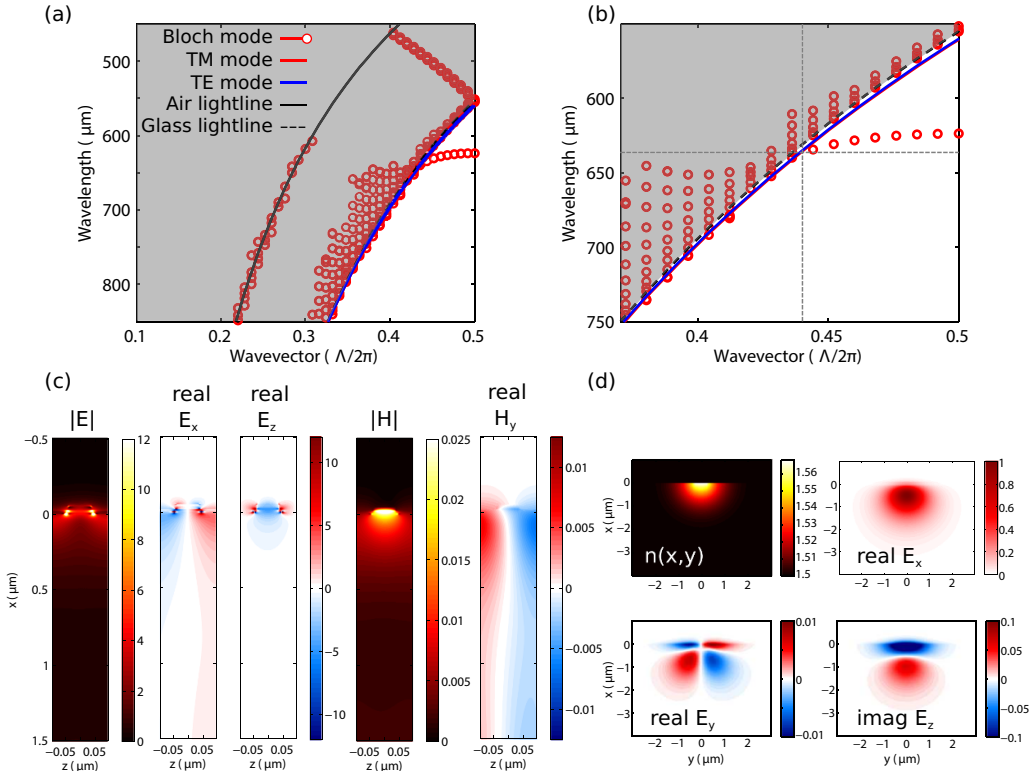


Figure 2. Modal analysis of the isolated waveguides. (a) Calculated dispersion relation of both the isolated IExWG and gold nanowires on glass ($\Lambda = 185$ nm). (b) Zoom of the dispersion relation around the phase matching condition. The gray dashed lines indicate the crossing point. (c) Distribution of the electric and magnetic fields and nonzero field components at $\lambda = 637.2$ nm with $k = 0.438(\Lambda/2\pi)$. (d) Distribution of the index profile and electric field components of the IExWG TM mode at $\lambda = 637.2$ nm with $n_{\text{eff}}k_0 = 14.874 \mu\text{m}^{-1}$.

the z direction with Bloch periodic boundary conditions while a supercell of seven cells was used in the y direction. PML boundary conditions were used in the x and y directions. An override mesh 3 nm along the x , y was used around the AuNW. The Au permittivity was fitted from spectroscopy ellipsometry (see appendix A).

In figure 2, we present the calculated dispersion relation for the isolated IExWG and periodic array of Au nanowires on glass. We also plotted the mode profile of the array mode and the TE and TM modes of the IExWG. The dispersion for the IExWG is close to the glass substrate light line. The cutoff frequencies for the fundamental TM and TE modes are 758 and 803 nm, respectively. The band of the Au NW mode is also close to the substrate light line but starts to deviate at around 670 nm. It is clearly a band mode that can propagate along the z -axis in a similar way to a SPP as a result of the wavevector conservation. The NW mode and the TM mode match their respective wavevectors and frequencies, which allows mode field interaction in a coupled waveguide at $k = 0.438(\Lambda/2\pi)$ and $\lambda = 637.2$ nm (gray dashed line in figure 2(b)). The NW and TM modes (i.e. main component E_x) are odd modes as they have mirror symmetry through $x = 0$. Finally, we calculated the dispersion of the coupled system (figure 3).

An anti-crossing point at $k = 0.438(\Lambda/2\pi)$ is obtained where energy exchange between the individual waveguide modes takes place. This anti-crossing point is a signature

of strong coupled modes in highly nonidentical parallel waveguides [26–30]. In addition to the dispersion relations, we calculated the excitation of a periodic array of Au nanowires of top of an IExWG with the TE and TM modes of the IExWG (figures 3(c) and (d)). Clearly, the TE mode does not interact with the array mode whereas the TM mode efficiently excites the array mode as observed in the electric field distribution across the yz -plane at $x_0 = 35$ nm (i.e. at the mid height of the AuNW). Finally, the influence of the period on the absorption properties of the NW on glass was investigated. Maximum absorption is achieved at $\Lambda = 150$ nm (see appendix A).

2.2. Fabrication and characterization of the structure

The gold nanowires were fabricated with the use of EBL on top of ion exchange glass waveguides.

We start with the fabrication of the optical glass waveguides with a technology developed at Teem Photonics [31]. Following the model described above (section 2.1), we thermally diffused silver/sodium ions on a glass substrate ($n_{\text{sub}} = 1.503$) through diffusion windows of $1.5 \mu\text{m}$. The diffusion window was previously obtained through photolithography process. The exchange temperature was thus fixed to 603 K and the exchange time to 4 min. After the fabrication of the optical waveguides, we transferred the array pattern on top of the IExWG chip with the use of EBL. Poly(methyl methacrylate) was used as EBL resist with a thickness of around 160 nm.

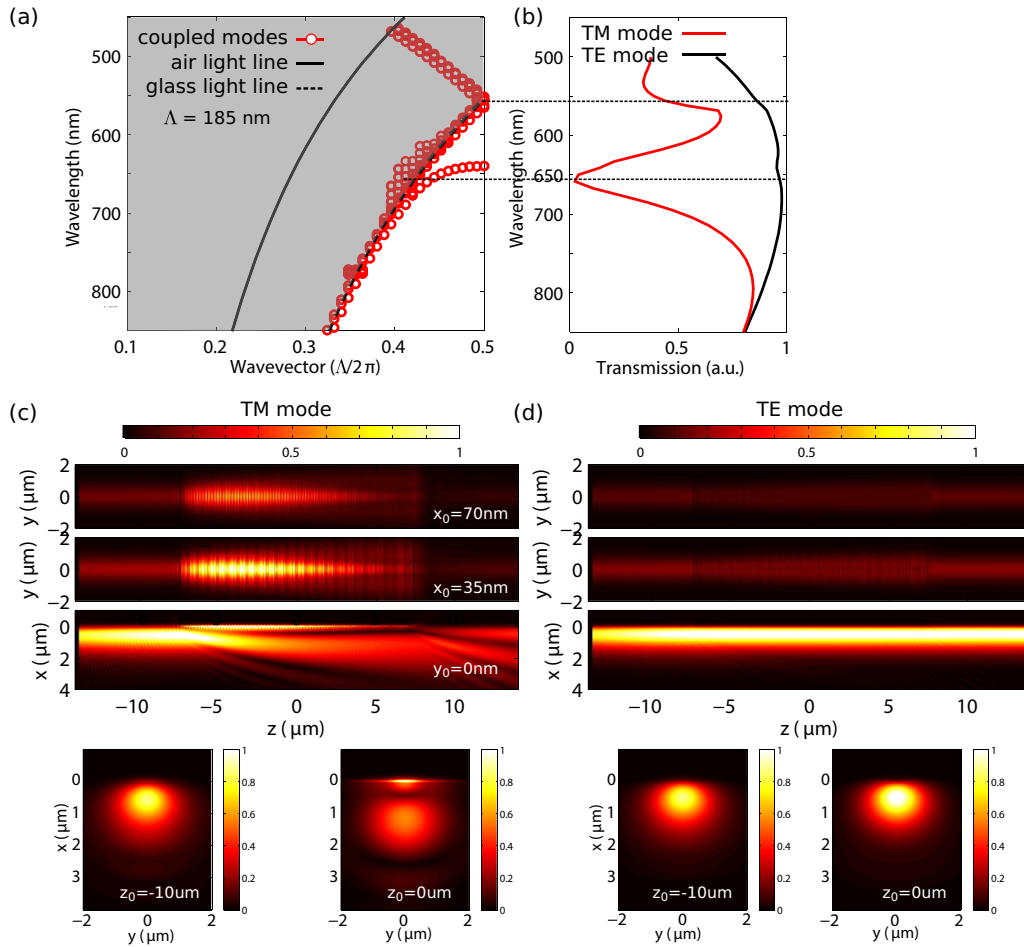


Figure 3. Modal analysis and propagation for the coupled system. (a) Calculated dispersion relation of the coupled waveguides (Au NW with period $\Lambda = 185$ nm). (b) Calculated transmission spectrum across the IExWG with the periodic array of gold nanowires on top. (c) Distribution of the electric and magnetic fields and non-zero field components at $\lambda = 637.2$ nm with $k = 0.438(\Lambda/2\pi)$. Distribution of the electric field across different planes on the integrated structure under the excitation with (c) TM and (d) TE modes of the IExWG.

To improve the resolution of the EBL, an intermediate layer of ITO of thickness $t_{ITO} = 20 \pm 4$ nm was deposited on the surface of the glass waveguides. Additionally, we conducted a resist descum to remove the residual resist scum left on the developed area. Oxygen plasma was used for an etch time of 5 s. The process ends with the thermal deposition of gold by Joule effect evaporation process and lift-off in acetone for 24 h. The thickness of the gold nanowires was $h_x = 30$ nm with average width $w_z = 75$ nm, and length $L_y = 50 \mu\text{m}$. The length of the nanowires is much larger than that of the IExWG diffusion window and therefore, can be considered as invariant along the y direction. Figure 4 presents scanning electron microscope images of the fabricated structure with nanowire period of $\Lambda = 185 \pm 15$ nm. Although the ITO layer improves the spatial resolution of the pattern transfer, period below 150 nm were not possible to obtain with our current EBL process.

We characterized the structure in both the far- and the near-field with transmission spectroscopy and an apertureless near-field scanning optical microscope (sNSOM) in tapping mode, respectively.

For the far-field measurements, we used a supercontinuum laser source (Fianium SC-450-4) covering a spectral

range ranging from 500 to 2100 nm. Light from this source was coupled to a single-mode polarization maintaining fiber (Thorlabs PM630-HP) connected to a pigtailed three-stages polarization rotator and then to a single-mode polarization maintaining micro-lensed fiber to couple light at the input facet of the waveguide. The transmitted signal was collected at the output facet of the IExWG with a multimode optical fiber (Thorlabs FG050LGA) plugged to a spectrometer (Ocean Optics Maya 2000Pro) operating in the spectral range from 550 to 1100 nm. The sample was mounted in an optical microscope stage assembled to a monochromatic CCD camera to observe its surface.

For the near-field measurements, we used a scattering NSOM equipped with an atomic force microscope tip made of silicon and working in tapping mode [32]. The laser source was a cw laser operating at wavelength $\lambda = 660$ nm. The source was coupled into the optical chip through a single-mode polarization maintaining micro-lensed fiber with an intermediate fiber polarization controller to excite the IExWG with its fundamental TM mode. We used a Hamamatsu APD module for the visible light detection (Hamamatsu APD module C12703). The sample here was mounted in a piezo-electric

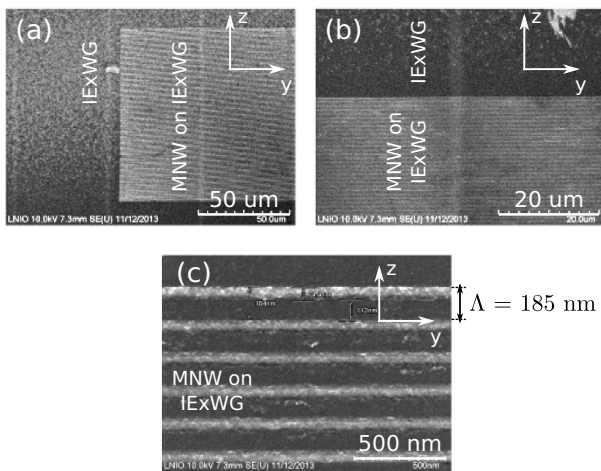


Figure 4. Periodic array of gold nanowires on glass waveguides made by ion exchange technology. (a) Scanning electron microscope image of an IExWG and a periodic array of Au NW on IExWG. (b) Zoom at the interface between an IExWG and the periodic array of Au NW on IExWG. (c) Zoom around the array with $\Lambda = 185 \pm 15$ nm and width 75 ± 15 nm.

stage for raster scanning across the yz -plane. The scattered field was modulated by the oscillation frequency of the AFM probe and therefore, we obtained the NSOM signal with the use of a lock-in amplifier that demodulates the scattered signal.

3. Results and discussion

Under TM mode illumination (light mainly polarized along the x direction), the periodic array of gold nanowires is excited, in contrast to the excitation with the TE mode (light mainly polarized along the y direction) (figure 5).

The transmission spectra for the TE (red dotted curve) and TM (blue dotted curve) modes, measured at the output facet of the ion exchange waveguide and normalized to light transmitted through a reference ion exchange waveguide without nanowires, are plotted in figure 5(c). For the TE mode, it is observed a minimum depth centered around the cut-off wavelength of the TM mode (green dashed line at $\lambda_{c, TM_0} = 767$ nm), because guided light was partially TM polarized. For the TM mode, a broadband peak appears with a minimum value around $\lambda_{LSP} = 665$ nm, which corresponds to the excitation of LSPRs in the nanowires. We notice that none of the two peaks correspond to Bragg reflections. Indeed, for a period of $\Lambda = 185$ nm, the effective index of the guided mode of $n_{wg} = 1.57$ (the highest possible value that TE or TM modes) and therefore, the first Bragg order ($m = 1$) occurs at $\lambda_{Bragg} = 2n_{eff}\Lambda/m = 580.9$ nm. To verify these results, we numerically computed the transmission spectra. Because of limited computational resources, only 81 nanowires were used and placed on top of the ion exchange waveguide with fixed width, height and period. As can be observed, the transmission spectrum for TE mode (red continuous curve) does not exhibit transmission losses. For the TM mode, the calculated spectrum exhibits a

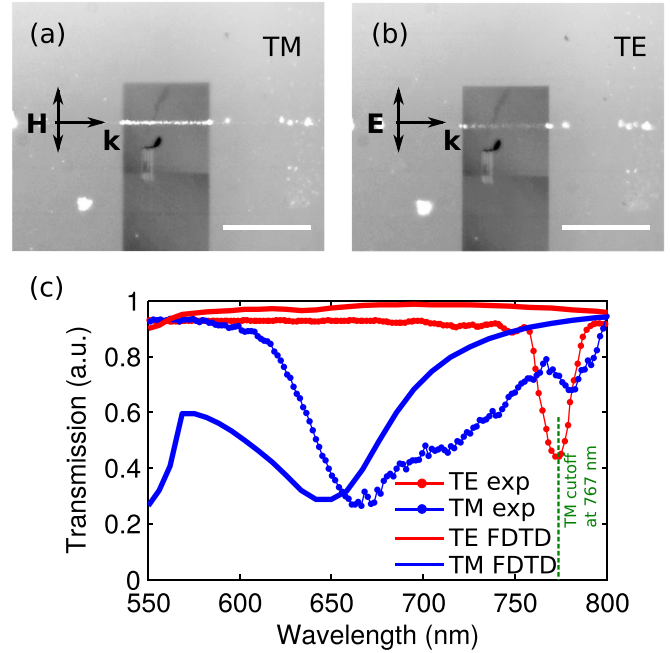


Figure 5. Far-field characterization of a periodic array of gold nanowires on IExWG. Optical microscope image of the surface of the device for excitation with (a) the TM and (b) TE modes of the IExWG. The coupled LSPRs of the array are only excited with the TM mode. (c) Normalized transmission spectra measured at the output of the IExWG for the TE (red dotted) and TM (blue dotted) modes. The minimum for the TM mode around $\lambda = 665$ nm corresponds to the excitation of the coupled LSPRs. FDTD transmission curves for TE (red solid line) and TM (blue solid line) modes with $N = 81$ nanowires.

broadband depth around $\lambda_{LSP} = 658$ nm, close to the experimental result. Mode conversion between TM and TE modes is less than 0.5% in transmission.

In figure 6, we present the simultaneously measured topography and optical near-field signal obtained with the scattering NSOM technique.

The horizontal white dotted lines in the topography indicates the position of the IExWG underneath the periodic array of Au nanowires. The near-field map clearly shows the field propagation along the structure, being observed a pattern of oblique fringes resulting from the interference between the field mode propagating through the structure and the field backscattered by the AFM probe. A spatial fast Fourier transform (FFT) analysis in three different regions of the intensity map (M1, M2 and M3) was performed to reveal the wavevectors of the optical modes (see appendix A). The M1 zone is along the IExWG, M2 along the transition from the IExWG to the array, and M3 a zone where no transition is present (figure 6).

From this FFT analysis was identified a spatial frequency that remained unchanged in the three regions corresponding to the TM mode of the waveguide, with an effective index $n_{eff, TM_0} = 1.496 \pm 0.073$. Only in region M2 did we observed two more frequencies corresponding to a mode radiating into the air ($n_{eff, sup} = 1.058 \pm 0.073$) and to a leaky mode radiating into the substrate ($n_{eff, sub} = 1.35 \pm 0.073$).

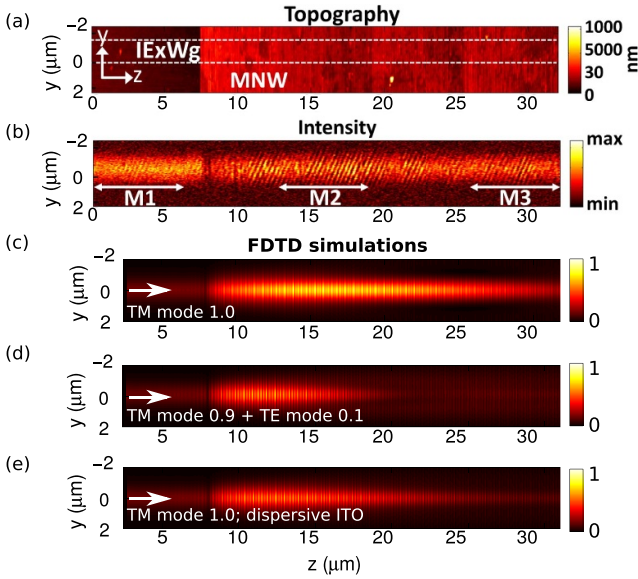


Figure 6. Scattering near-field scanning optical microscopy characterization. (a) Topography and (b) intensity near-field maps of light propagating through the integrated device with array period of $\Lambda = 185 \pm 15$ nm. The interaction zone is clearly seen as light propagates through the coupling region M2. FDTD simulations of the structure at $\lambda = 660$ nm with (c) the TM mode, (d) the 0.9 TM + 0.1 TE modes, and (e) the TM mode with dispersive ITO.

Discrepancies between numerical and experimental results could arise from the following situations. Firstly, even though we used a fiber polarization controller, it was not possible to fully separate the TM and TE modes. A simulation of this latter situation is plotted in figure 6(d), where 90% TM mode + 10% TE mode were used. Secondly, our experimental ITO presents absorption that was not taken into account in simulations. In figure 6(e) we did the simulation with dispersive ITO (see appendix A). In addition, fabrication imperfections give rise to scattering loss that potentially could lead to mode conversion between the two photonic modes [33, 34].

To achieve control of the mode coupling between the TM mode and array mode, the period can be either reduced or increased in order to shift the coupled LSPRs [35]. For instance, considering a shorter period $\Lambda = 100$ nm (with the same width for the nanowires and width $w_z = 75$ nm, the dispersion curves show that the antisymmetric coupled mode is coupled to radiative mode as its band lies above the substrate light-line. In contrast, the symmetric coupled mode is guided as its band lies below the IExWG light line at wavevector at $k = 0.212(\Lambda/2\pi)$. The electric and magnetic field components are also plotted in figure 7.

This coupling results in a mode coupling that leads to an energy exchange between the photonic and plasmonic modes (figure 7). The fabrication of a short period array of MNW on top of a dielectric waveguide, like the one we present, is a challenging situation due to charge accumulation in the substrate, its experimental demonstration remaining as an open task. Currently, periods below 150 nm are difficult to achieve consistently.

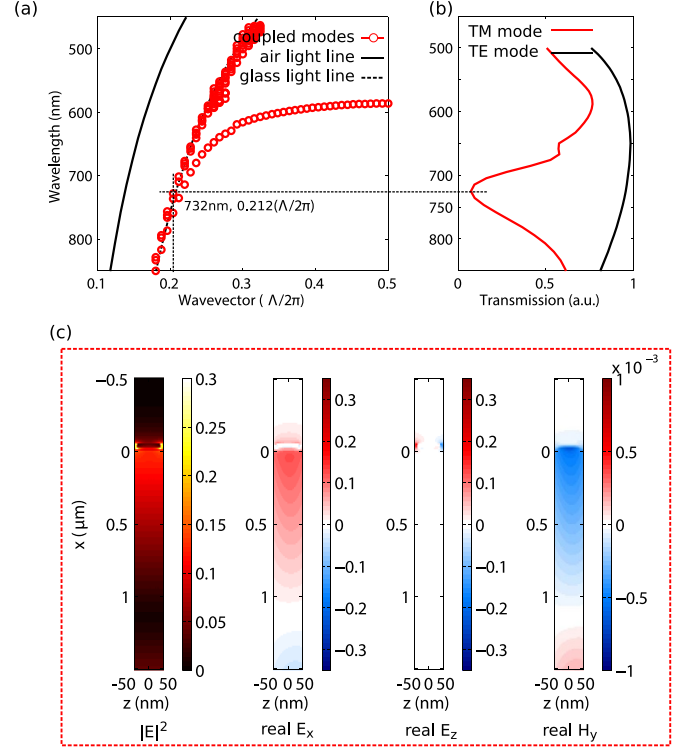


Figure 7. Modal analysis and propagation for the coupled system. (a) Calculated dispersion relation of the coupled waveguides (Au NW with period $\Lambda = 100$ nm). (b) Calculated transmission spectrum across the IExWG with the periodic array of Au nanowires on top. Distribution of the electric and magnetic field components at $k = 0.212(\Lambda/2\pi)$ for the coupled guided mode.

4. Conclusion

We experimentally demonstrated the excitation of coupled LSPRs of a subdiffractive periodic array of gold nanowires on an optical glass waveguide fabricated with ion exchange technology. The array was fabricated with the use of EBL and lift-off processes. Coupled LSPRs, named array mode, arises from the coupling between the LSPR of the individual nanowires. According to the period, the array mode can be efficiently excited with the TM mode of the ion exchange waveguide. The resonance frequency of the array mode can be tuned with the period of the array, however, the fabrication of an array with a period below 150 nm remains a challenge with current EBL and lift-off processes. The integrated optical device on ion exchange technology operates across the visible spectrum and integrates in a straightforward manner with commercial optical fibers.

Acknowledgments

Numerical calculations were performed with the resources of the French regional Grand-Est HPC Center ROMEO. The fabrication was done at the French Regional Grand Est nanofabrication and nanocharacterization platform (Nano'Mat). The authors thank Consejo Nacional de Ciencia

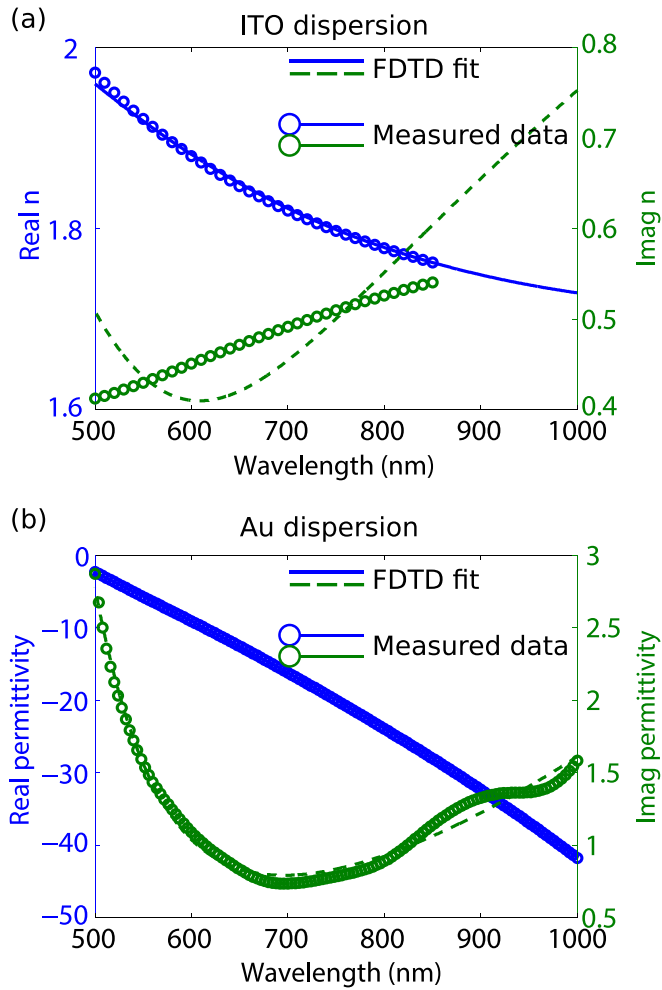


Figure A1. Measured and fit results for the material dispersion. Material dispersion of (a) the ITO (figures 6(e) and (b)) gold nanowires. Blue solid lines and green dashed lines are FDTD fit results. Circles are measured data by ellipsometric spectroscopy.

y Tecnología (CONACYT, Basic Scientific Research Grant No. A1-S-21527) for partial financial support.

Appendix A. Materials dispersion

We measured the material dispersion of the ITO (figure 6(e)) and Au with the use of ellipsometry spectroscopy (Horiba Yobin) in a spectral range of 500 – 850 nm. The results of the FDTD fit performed with FDTD solutions by Lumerical are presented in figure A1.

A.1. Influence of the period on the absorption properties of the metallic nanowires

The absorption properties of the nanowires was investigated numerically as a function of the period array. A TM polarized plane wave illuminates the array of nanowires from the substrate at grazing angle $\theta = 84^\circ$. Bragg order are

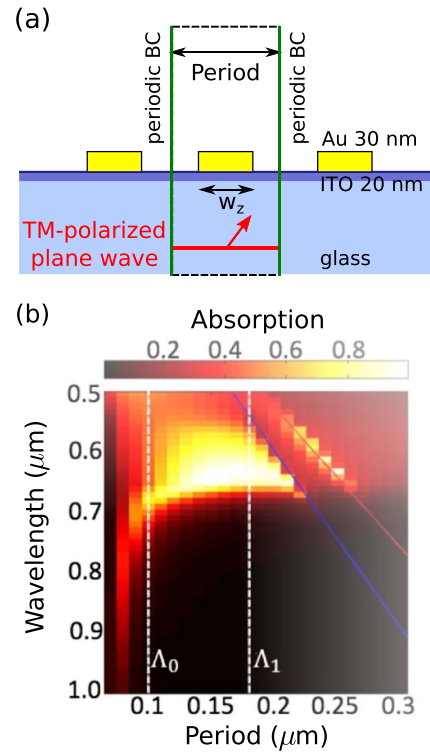


Figure A2. Influence of the period on the absorption properties on an array on gold nanowires on glass. (a) Scheme of the geometry and illumination configuration (TM polarized light at grazing angle $\theta = 84^\circ$). An ITO layer separates the MNW from the glass substrate. (b) Absorption is maximum at a period 150 nm. Blue and red solid lines are Bragg orders.

clearly obtained as well as an optimum absorption value at $\Lambda = 150$ nm.

A.2. FFT analysis

From the interference pattern of the NSOM intensity map (figure 6(b)), and following [32], the wavevectors of the optical modes propagating in the structure can be deduced by means of the FFT.

The images in figure A3 show the spatial FFT across the regions M1, M2, and M3 of figure 6(b). The spatial frequency that remains unchanged in the three images (marker P1), corresponds to the TM mode of the IExWG. The effective index of the mode was computed via $n_{\text{eff}} = \lambda/\nu$, where $\lambda = 660$ nm is the wavelength of the incident light and ν is the measured spatial frequency. In all regions the effective index of the TM mode was $n_{\text{eff, TM}_0} = 1.496 \pm 0.073$. Two more frequencies were observed in region M2, close to the TM mode frequency (marker P1). The frequency P2 showed an effective index $n_{\text{eff, sup}} = 1.058 \pm 0.073$, close to the free-space index and thus, a radiated mode (air). The spatial frequency P3 exhibited an effective index $n_{\text{eff, rad}} = 1.35 \pm 0.073$, which is lower than the index of the substrate ($n_{\text{sub}} \approx 1.49$), thus it was identified as a leaky mode radiating into the substrate. Because the period of the MNW is too short to allow diffraction orders, both, P2 and P3 resonances are only excited at the input of the

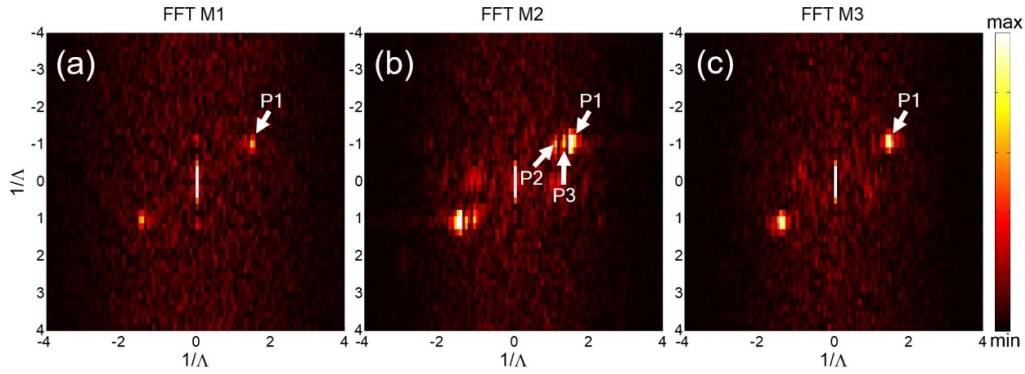


Figure A3. FFT analysis. Spatial FFT across regions (a) M1, (b) M2, and (c) M3 of figure 6(b). The arrows point the location of the TM mode (P1) with an effective index $n_{\text{eff}} = 1.496 \pm 0.073$. In region M2, the FFT map exhibits two resonances corresponding to modes radiated into the air (P2) and substrate (P3).

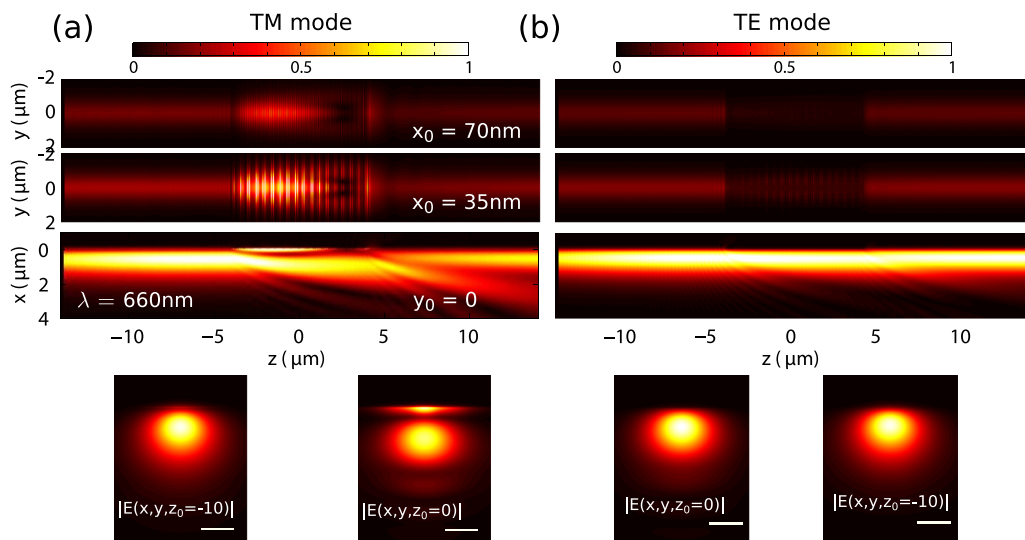


Figure A4. Propagation on an integrated structure with MNW array of period $\Lambda = 100$ nm. Distribution of the electric field across different planes on the integrated structure with $\Lambda = 100$ nm under the excitation with (a) the TM and (b) the TE modes.

grating and decouple after a few microns in the MNW region, and they no longer appear in region M3.

A.3. Propagation on a integrated structure with MNW array of period $\Lambda = 100$ nm

In figure A4 we present the distribution of the electric field across different planes on the integrated structure with array period of $\Lambda = 100$ nm under the excitation with (a) the TM and (b) the TE modes. The electric field maps are taken at wavelength $\lambda = 732$ nm.

The coupling length is decrease compared to that for a periodic array of MNPs with period $\Lambda = 185$ nm. Electric field

is also enhanced, however, as mentioned in the manuscript, the fabrication, specifically the EBL, is a challenging situation for this periodic array due to charge accumulation in the substrate.

A.4. Integrated structure with MNW array of period $\Lambda = 100$ nm

As shown in section A.4, the coupling efficiency can be reached with the control of the period of the array. At this period, higher order modes of the array are supported at shorter wavelengths. Figure A5 presents the dispersion relation of such a mode and the distribution of the electric and magnetic field components at wavevector $k = 0.5(\Lambda/2\pi)$.

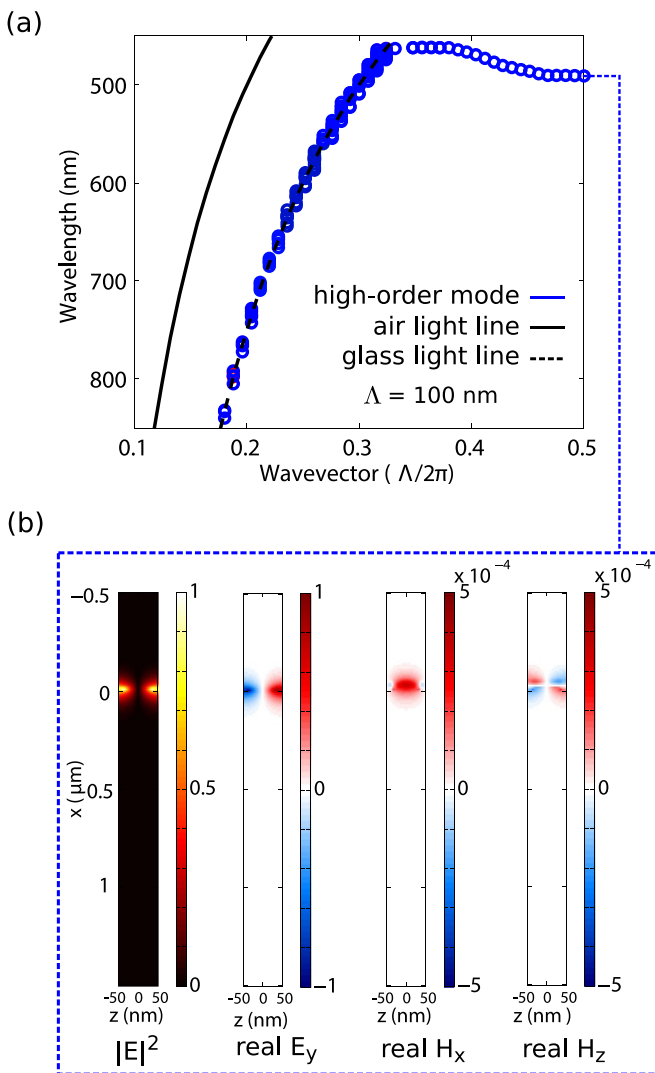


Figure A5. Modal analysis and propagation for the coupled system. (a) Calculated dispersion relation of the coupled waveguides (Au NW with period $\Lambda = 100$ nm). (b) Distribution of the electric and magnetic field components at $k = 0.5(\Lambda/2\pi)$ for the guided higher-order mode of the array of metallic nanowires.

ORCID iD

Ricardo Tellez-Limon  <https://orcid.org/0000-0002-8028-9216>

References

- [1] Novotny L and Hecht B 2009 *Principles of Nano-Optics* 2nd edn (Cambridge: Cambridge University Press) ch 12, pp 369–413
- [2] Quinten M, Leitner A, Krenn J R and Aussenegg F R 1998 Electromagnetic energy transport via linear chains of silver nanoparticles *Opt. Lett.* **23** 1331–3
- [3] Hochman A and Leviatan Y 2009 Rigorous modal analysis of metallic nanowire chains *Opt. Express* **17** 13561–75
- [4] Compaijen P J, Malyshev V A and Knoester J 2015 Engineering plasmon dispersion relations: hybrid nanoparticle chain-substrate plasmon polaritons *Opt. Express* **23** 2280–92
- [5] Dong J-W and Deng Z-L 2013 Direct eigenmode analysis of plasmonic modes in metal nanoparticle chain with layered medium *Opt. Lett.* **38** 2244–6
- [6] Weber W H and Ford G W 2004 Propagation of optical excitations by dipolar interactions in metal nanoparticle chains *Phys. Rev. B* **70** 125429
- [7] Fung K H and Chan C T 2007 Plasmonic modes in periodic metal nanoparticle chains: a direct dynamic eigenmode analysis *Opt. Lett.* **32** 973–5
- [8] Yan M 2019 Complex- k modes of plasmonic chain waveguides *J. Phys. Commun.* **3** 115015
- [9] Barnes W L, Dereux A and Ebbesen T W 2003 Surface plasmon subwavelength optics *Nature* **424** 824
- [10] Quidant R, Girard C, Weeber J-C and Dereux A 2004 Tailoring the transmittance of integrated optical waveguides with short metallic nanoparticle chains *Phys. Rev. B* **69** 085407
- [11] Maier S A and Atwater H A 2005 Plasmonics: localization and guiding of electromagnetic energy in metal/dielectric structures *J. Appl. Phys.* **98** 011101
- [12] Lesuffleur A, Im H, Lindquist N C and Oh S-H 2007 Periodic nanohole arrays with shape-enhanced plasmon resonance as real-time biosensors *Appl. Phys. Lett.* **90** 243110
- [13] Mokkaapati S, Beck F J, Polman A and Catchpole K R 2009 Designing periodic arrays of metal nanoparticles for light-trapping applications in solar cells *Appl. Phys. Lett.* **95** 053115
- [14] Valsecchi C and Brolo A G 2013 Periodic metallic nanostructures as plasmonic chemical sensors *Langmuir* **29** 5638–49
- [15] Février M et al 2012 Giant coupling effect between metal nanoparticle chain and optical waveguide *Nano Lett.* **12** 1032–7
- [16] Tellez-Limon R, Février M, Apuzzo A, Salas-Montiel R and Blaize S 2014 Theoretical analysis of Bloch mode propagation in an integrated chain of gold nanowires *Photon. Res.* **2** 24–30
- [17] Tellez-Limon R, Février M, Apuzzo A, Salas-Montiel R and Blaize S 2017 Numerical analysis of tip-localized surface plasmon resonances in periodic arrays of gold nanowires with triangular cross section *J. Opt. Soc. Am. B* **34** 2147–54
- [18] Krasnokutska I, Chapman R J, Tambasco J-L J and Peruzzo A 2019 High coupling efficiency grating couplers on lithium niobate on insulator *Opt. Express* **27** 17681–5
- [19] Bellegarde C, Dirani H E, Letartre X, Petit-Etienne C, Monat C, Hartmann J-M, Sciancalepore C and Pargon E 2019 Technological advances on Si and Si₃N₄ low-losses waveguide platforms for nonlinear and quantum optics applications *Proc. SPIE* **10933** 1039903
- [20] Ma M, Park A H K, Wang Y, Shoman H, Zhang F, Jaeger N A F and Chrostowski L 2019 Sub-wavelength grating-assisted polarization splitter-rotators for silicon-on-insulator platforms *Opt. Express* **27** 17581–91
- [21] Tellez-Limon R, Blaize S, Gardillou F, Coello V and Salas-Montiel R 2020 Excitation of surface plasmon polaritons in a gold nanoslab on ion-exchanged waveguide technology *Appl. Opt.* **59** 572–8
- [22] Tervonen A, Honkanen S K and West B R 2011 Ion-exchanged glass waveguide technology: a review *Opt. Eng.* **50** 50–16
- [23] Broquin J-E 2001 Ion-exchanged integrated devices *Proc. SPIE* **4277** 1–13
- [24] Choo P Y, Frantz J A, Carriere J T A, Mathine D L, Kostuk R K and Peyghambarian N 2003 Measurement and modeling of ion-exchange parameters for IOG-10 glass *Opt. Eng.* **42** 2812–16
- [25] Wang B, Blaize S, Seok J, Kim S, Yang H and Salas-Montiel R 2019 Plasmonic-based subwavelength graphene-on-hBN modulator on silicon photonics *IEEE J. Sel. Top. Quantum Electron.* **25** 1–6

- [26] Hardy A and Streifer W 1985 Coupled mode theory of parallel waveguides *J. Lightwave Technol.* **3** 1135–46
- [27] Li H, Chen B, Qin M and Wang L 2020 Strong plasmon-exciton coupling in mim waveguide-resonator systems with WS2 monolayer *Opt. Express* **28** 205–15
- [28] Li H, Qin M, Ren Y and Hu J 2019 Angle-independent strong coupling between plasmonic magnetic resonances and excitons in monolayer WS2 *Opt. Express* **27** 22951–9
- [29] Li H, Ji C, Ren Y, Hu J, Qin M and Wang L 2019 Investigation of multiband plasmonic metamaterial perfect absorbers based on graphene ribbons by the phase-coupled method *Carbon* **141** 481–7
- [30] Rodriguez S R-K 2016 Classical and quantum distinctions between weak and strong coupling *Eur. J. Phys.* **37** 025802
- [31] Teem-Photonics (www.teemphotonics.com/integrated-optics/custom-photonics-circuits/)
- [32] Blaize S, Aubert S, Bruyant A, Bachelot R, Lerondel G, Royer P, Broquin J-E and Minier V 2003 Apertureless scanning near-field optical microscopy for ion exchange channel waveguide characterization *J. Microsc.* **209** 155–61
- [33] Tellez-Limon R, Bahari B, Hsu L, Park J-H, Kodigala A and Kanté B 2016 Integrated metaphotonics: symmetries and confined excitation of LSP resonances in a single metallic nanoparticle *Opt. Express* **24** 13875–80
- [34] Espinosa-Soria A, Pinilla-Cienfuegos E, Díaz-Fernández F J, Griol A, Martí J and Martínez A 2018 Coherent control of a plasmonic nanoantenna integrated on a silicon chip *ACS Photonics* **5** 2712–17
- [35] Noguez C 2007 Surface plasmons on metal nanoparticles: the influence of shape and physical environment *J. Phys. Chem.* **111** 3806–19